Relationship between intracellular pH and proton mobility in rat and guinea-pig ventricular myocytes

Pawel Swietach and Richard D. Vaughan-Jones

Burdon Sanderson Cardiac Science Centre, University Laboratory of Physiology, Oxford OX1 3PT, UK

Intracellular H^+ ion mobility in eukaryotic cells is low because of intracellular buffering. We have investigated whether H_i^+ mobility varies with pH_i. A dual microperfusion apparatus was used to expose guinea-pig or rat myocytes to small localized doses (3–5 mM) of ammonium chloride (applied in Hepes-buffered solution). Intracellular pH (pH_i) was monitored confocally using the fluorescent dye, carboxy-SNARF-1. Local ammonium exposure produced a stable, longitudinal pH_i gradient. Its size was fed into a look-up table (LUT) to give an estimate of the apparent intracellular proton diffusion coefficient (D_H^{app}). LUTs were generated using a diffusion–reaction model of H_i^+ mobility based on intracellular buffer diffusion. To examine the pH_i sensitivity of D_H^{app}, whole-cell pH_i was initially displaced using a whole-cell ammonium or acetate prepulse, before locally applying the low dose of ammonium. In both rat and guinea-pig, D_H^{app} decreased with pH_i over the range 7.5–6.5. In separate pipette-loading experiments, the intracellular diffusion coefficient for carboxy-SNARF-1 (a mobile-buffer analogue) exhibited no significant pH_i dependence. The pH_i sensitivity of D_H^{app} is thus likely to be governed by the mobile fraction of intrinsic buffering capacity. These results reinforce the buffer hypothesis of H_i^+ mobility. The pH_i dependence of D_H^{app} was used to characterize the mobile and fixed buffer components, and to estimate D_{mob} (the average diffusion coefficient for intracellular mobile buffer). One consequence of a decline in H_i^+ mobility at low pH_i is that it will predispose the myocardium to pH_i nonuniformity. The physiological relevance of this is discussed.

(Received 4 March 2005; accepted after revision 26 May 2005; first published online 26 May 2005)
Corresponding author R. D. Vaughan-Jones: Burdon Sanderson Cardiac Science Centre, University Laboratory of Physiology, Oxford OX1 3PT, UK. Email: richard.vaughan-jones@physiol.ox.ac.uk

Changes of intracellular pH (pH_i) exert powerful effects on contraction and excitation in the heart (Allen & Orchard, 1983; Bountra & Vaughan-Jones, 1989; Orchard & Kentish, 1990; Harrison *et al.* 1992; Choi *et al.* 2000). For this reason, pH_i is regulated by acid/base transporters expressed at the sarcolemma (Lagadic-Gossmann *et al.* 1992; Leem *et al.* 1999). In addition, diffusive mechanisms regulate pH_i spatially within the cell (Swietach & Vaughan-Jones, 2005; Vaughan-Jones *et al.* 2006). The importance of spatial control has been highlighted recently by the finding that intracellular H^+ mobility is low, the apparent H_i^+ diffusion coefficient (D_H^{app}) in ventricular myocytes being up to 300-fold lower (Vaughan-Jones *et al.* 2002; Zaniboni *et al.* 2003) than in water (Vanysek, 1999). A similarly low D_H^{app} has been estimated in murine enterocytes (Stewart *et al.* 1999) and snail neurones (Swietach *et al.* 2003).

It has been proposed that H_i^+ diffusion is limited by intracellular buffers, which bind the majority of acid or base within a cell (Junge & McLaughlin, 1987; Irving *et al.* 1990; Al-Baldawi & Abercrombie, 1992; Vaughan-Jones *et al.* 2002; Swietach *et al.* 2003). According to the buffer hypothesis of H_i^+ mobility, D_H^{app} can be expressed in terms of the mobile buffer diffusion coefficient (D_{mob}) and the mobile-to-total buffering capacity ratio (ϕ):

$$D_H^{app} = D_{mob}\frac{\beta_{mob}}{\beta_{total}} = D_{mob}\phi \quad (1)$$

Because the capacity of a cellular buffer is defined in part by its pK ($-$log of dissociation constant), it will vary with pH_i. Consequently the value for D_H^{app} is also predicted to vary (e.g. Zaniboni *et al.* 2003). So far, this hypothesis has been tested on extracted samples of molluscan axoplasm only (Al-Baldawi & Abercrombie, 1992), where H_i^+ mobility increased threefold when the ambient pH was raised from about 6.6 to >8.2. The nature of buffering in molluscan axoplasm and in an intact mammalian myocyte is likely to differ considerably, and so we have measured D_H^{app} in guinea-pig and rat cardiomyocytes over a range of pH_i values. We have done this by using a dual microperfusion apparatus that exposes one end of an isolated cell to a solution containing ammonium chloride (i.e. a salt of the membrane-permeant weak base, NH_3). This

 DOI: 10.1113/jphysiol.2005.086165

sets up an intracellular longitudinal pH_i gradient as NH_3 enters the cell, raising pH_i locally at the exposed end. Because H_i^+ mobility is low, the pH_i gradient is not collapsed by diffusive flow of H^+ ions from the unexposed end. The amplitude of the steady-state gradient is related mathematically to the value of D_H^{app} (Swietach *et al.* 2005*a*). By performing dual microperfusion at different average levels of pH_i, a variation of D_H^{app} with pH_i was detected. We have considered whether this is related to pH_i-dependent changes of mobile (β_{mob}) and fixed (β_{fix}) buffering capacity, and D_{mob}. In order to examine the last possibility, we investigated the effect of changing pH_i on the mobility of intracellular carboxy-SNARF-1 introduced locally from a cell-attached micropipette. Because carboxy-SNARF-1 has a pK in the physiological range (pK ~7.6), and its molecular mass is comparable with typical intracellular mobile buffers (cf. Vaughan-Jones *et al.* 2002), its diffusive properties serve as a useful model for the behaviour of intrinsic mobile buffer.

The importance of pH_i-sensitive H_i^+ mobility to the spatial regulation of pH_i and to the homeostasis of cardiomyocyte function is discussed.

Methods

Myocyte isolation

Rat and guinea-pig ventricular myocytes were enzymically isolated in a Langendorff perfusion set-up, as previously described (e.g. Lagadic-Gossmann *et al.* 1992; Zaniboni *et al.* 2003). Briefly, using a combination of enzymic and mechanical dispersion at 37°C, single ventricular myocytes were isolated from ~450 g albino Dunkin Hartley guinea-pigs and ~300 g Sprague-Dawley rats (killed by cervical dislocation according to UK Home Office regulations). Rat myocytes were digested using Liberase 3 (a mixture of collagenase I and II, and protease; 0.2 mg ml^{-1}; Roche Diagnostics, UK) for 12 min. Guinea-pig myocytes were digested using a combination of collagenase P (0.23 mg ml^{-1}; Roche Diagnostics) and protease (0.04 mg ml^{-1}; Sigma, UK) for 10–15 min. The cells were finally suspended in Hepes-buffered Dulbecco's modified Eagle's medium (Sigma, UK) at pH 7.4, and kept at room temperature until use. Experiments were performed on rod-shaped myocytes that did not contract spontaneously.

Solutions, drugs and fluorophore

Superfusion solutions were delivered at ~2 ml min^{-1} by means of a peristaltic pump to a 1 ml capacity Plexiglass superfusion chamber, mounted on the stage of an inverted microscope (Leica DM IRBE, Germany). The temperature of the superfusates was kept at 37°C by an electrical temperature control circuit. Before each experiment, the bottom of the bath was coated with 200 μl of 1% poly L-lysine (Sigma, UK) to promote cell adhesion. After a period of 3 min, poly L-lysine was washed away with the superfusion solution, and the cell suspension could then be applied. When required, microperfusion solutions were delivered using a double-barrelled square-bore micropipette (see Spitzer *et al.* 2002 and Swietach *et al.* 2005*a* for details of assembly and use).

Hepes-buffered normal Tyrode solution contained (mM): 135 NaCl, 4.5 KCl, 1 $MgCl_2$, 2 $CaCl_2$, 11 glucose, 20 Hepes. Solutions containing 3, 5 or 30 mM ammonium chloride, 80 mM sodium acetate or 15 mM trimethylamine (TMA) were made by adding the weak acid or weak base to a normal Tyrode solution, which had an appropriately reduced NaCl concentration to keep osmolarity constant. During dual microperfusion, in order to visualize the boundary between the two microstreams, 20 mM sucrose was included in one microstream (the one containing 3–5 mM NH_4Cl). Inclusion of sucrose has minimal effect on cell physiology (Spitzer *et al.* 2000). The pH of all solutions was adjusted to pH 7.4 with 4 M NaOH at 37°C. In some experiments, 30 μM cariporide (a kind gift from Dr H. W. Kleemann of Sanofi-Aventis, Germany), a selective Na^+–H^+ exchanger (NHE-1) inhibitor (Scholz *et al.* 1995; Zaniboni *et al.* 2003), was added to the superfusates.

In experiments involving dual microperfusion, cells were loaded uniformly with the membrane-permeant acetoxymethyl (AM) ester of the fluorophore, carboxy-SNARF-1: 200 μl of cell suspension was incubated with 1.5 μl of carboxy-SNARF-1-AM (Molecular Probes, USA; prepared by dissolving 1 mg of the dye ester in 1 ml DMSO) for 8 min. In experiments measuring dye diffusion, the free-acid form of carboxy-SNARF-1 was loaded into cells via a cell-attached glass micropipette containing a solution of 400 μM dye, 140 mM KCl, 1 mM $MgCl_2$, 10 mM Hepes, at pH 7.1.

Confocal microscopy

The experimental set-up consisted of an inverted Leica confocal microscope supplied with Leica LCS software and a Leica ×40 oil-immersion planoapochromat objective lens (numerical aperture 1.25). Dye excitation was achieved with the 514 nm laser line of an air-cooled argon laser. Emitted fluorescence was simultaneously collected by two photomultiplier tubes equipped with band-pass filters at 640 ± 20 and 580 ± 20 nm. A transmitted light detector also provided a nonfluorescent image of the cell for measuring cell dimensions, and for locating the dual microstream boundary or the cell-attached micropipette. Images were acquired in 'x–y' two-dimensional scanning mode, at a rate of one frame every 2.1 s. Pinhole

Table 1. Physical and physiological constants in the computational model of dual microperfusion

Symbol	Definition	Value	Reference
η	Surface area increase due to membrane infolding	1.69 (gp); 2.14 (r)	Satoh *et al.* (1996); Soeller & Cannell (1998)
k_{buff}^{on}	Intrinsic buffer protonation rate constant	$\sim 10^{10}$ M^{-1} s^{-1} (at 37°C)	Eigen (1964)
k_{buff}^{on}	Ammonium protonation rate constant	4.3×10^{10} M^{-1} s^{-1} (at 37°C)	Eigen (1964)
K_{am}	Ammonium dissociation constant	$10^{-9.03}$	Leem *et al.* (1999)
D_H	Intracellular free-proton diffusion coefficient	6.05×10^{-5} cm^2 s^{-1}	Swietach *et al.* (2003)
D_{NH_3}, D_{NH_4}	Ammonia and ammonium diffusion coefficient	1.27×10^{-5} cm^2 s^{-1}	Swietach *et al.* (2003)
P_{NH_3}	Ammonia membrane permeability constant	54.5×10^{-4} cm s^{-1}	Swietach *et al.* (2005*a*)
P_{NH_4}	Ammonium membrane permeability constant	1.408×10^{-7} cm s^{-1}	Leem *et al.* (1999)
Rad	Cross-sectional cell radius	13.4 μm (gp); 12.7 μm (r)	This study
pK_i	Intrinsic buffer p*K* values for eqn (3)	7.574, 6.448, 6.10 (gp); 7.574, 6.448, 6.21 (r)	Based on Zaniboni *et al.* 2003)
C_i	Intrinsic buffer concentrations for eqn (3)	15.74, 13.06, 68.3 mM (gp); 15.74, 13.06, 62.13 mM (r)	Based on Zaniboni *et al.* 2003)

gp, guinea-pig; r, rat.

size was kept between 1 and 1.5 Airy units. In order to convert fluorescence recordings to intracellular pH, a macro was written for SCION Image (SCION Corp., USA) to perform background fluorescence subtraction and 580/640 nm image ratioing. The ratiometric signal was converted to pH_i using calibration curves obtained in separate experiments performed on guinea-pig and rat myocytes using the 'nigericin technique' (Thomas *et al.* 1979).

Dual microperfusion experiments and the computational algorithm

Single isolated guinea-pig and rat myocytes, AM-loaded with dye, were subjected to dual microperfusion with the microstream boundary usually positioned across the middle of the cell (Spitzer *et al.* 2000; Swietach *et al.* 2005*a*). The microstream was positioned approximately perpendicular to the myocyte (see, e.g. Fig. 2*Aa* or *Ba*). A low, 3–5 mM dose of NH_4Cl was present in one of the two microstreams. The other microstream contained the same solution as the superfusate (i.e. Hepes-buffered normal Tyrode solution). The result was a longitudinal pH_i gradient (between ~0.1 and ~0.6 pH units). The analytical procedure (see below) then permitted the assignment of a value for D_H^{app} to a particular pH_i, averaged over a given pH_i gradient.

A macro was designed to find the edges of the cell and place nine adjacent regions of interest (ROIs) along the longitudinal axis of a cell image. The width of each ROI was 75% of the cell width. The average pH among all nine ROIs was used to calculate cell-averaged pH_i. The end-to-end pH_i gradient was taken as the pH difference between the first and the ninth ROI. The size of this gradient depends, in part, on H_i^+ mobility (the lower the mobility, the larger the gradient). Details have been published (Swietach *et al.* 2005*a*) of a computational algorithm for estimating D_H^{app} from experimental measurements of the gradient. By using this algorithm, and by manipulating whole-cell pH_i prior to imposing dual microperfusion, it was possible to investigate the pH_i dependence of D_H^{app}.

Starting pH_i was manipulated by prior exposure of the *whole* cell to a prepulse of 30 mM ammonium or 80 mM acetate. On removal of the weak base or weak acid, pH_i was displaced in the acid and alkaline direction, respectively. The degree of pH_i displacement was varied by altering the duration of the prepulse (4–12 min). As shown in Swietach *et al.* (2005*a*), the sarcolemmal acid/base transporters do not significantly influence the size of the pH_i gradient seen during dual microperfusion. Nonetheless, in some experiments, particularly those involving a large acidosis, cariporide (30 μM) was included in both microstreams to inhibit Na^+-H^+ exchange (NHE).

The size of the longitudinal pH_i gradient is affected not only by H_i^+ mobility, but also by cell geometry, the dose and degree of cellular perfusion with ammonium (Spitzer *et al.* 2000; Swietach *et al.* 2005*a*), and, as hypothesized in the present work, by the starting value of pH_i. To account for variation in these factors, look-up tables (LUTs) were generated for rat and guinea-pig myocytes using diffusion–reaction algorithms instructed to calculate the size of the end-to-end pH_i gradient for a range of D_H^{app} values (2.5×10^{-7}–7.5×10^{-6} cm^2 s^{-1}), boundary positions (30–80% of cell length), cell lengths (80–180 μm) and starting pH_i (6.0–8.0). Because the width of a myocyte tends to vary less than its length, algorithms were run using an average value for width (see Table 1). By the reverse procedure, D_H^{app} could be deduced from LUTs using experimental data for the size of the longitudinal pH_i gradient, cell length, boundary position, ammonium concentration and starting pH_i.

The computational algorithm for predicting a longitudinal pH_i gradient includes terms for intracellular diffusion (buffer, NH_4^+, NH_3, free H^+), chemical reaction (H^+-buffering, reversible protonation of ammonia), and transmembrane permeation (NH_3 and NH_4^+). Figure 1 shows a schematic diagram summarizing the various components of diffusion, reaction and permeation. The algorithm was solved over a 60 s period using the MATLAB function 'pdepe' (Mathworks, USA). It was computed according to the function:

$$\frac{\partial u}{\partial t} = \nabla(D\nabla u) + R(u) + T(u) \qquad (2)$$

where u is the concentration of the participating solutes, D is the vector of their diffusion coefficients, R is a set of equations describing their intracellular reactions, and T is a set of transmembrane flux equations. A more detailed description of the computational algorithm is presented in the online supplement to the current paper.

In order to characterize H_i^+ mobility, the present work attempts to evaluate the characteristics of fixed and mobile buffer within the cell. Values for total intrinsic buffering capacity, β_{total} (i.e. the sum of fixed and mobile components), have been determined previously, and shown to depend on the value of pH_i, as illustrated, for example, in Fig. 5(C) of Zaniboni *et al.* (2003). For clarity, the data and best-fitting curve in that figure have been reproduced in Fig 5*A* and *B* of the present work (diamond symbols, light-grey curve). In the original work, the pH_i dependence of β_{total} was reproduced mathematically by using a family of 20 mobile buffers (identified from the literature) and a single fixed-buffer population. While trying to simplify this curve-fitting procedure in the present work, it was found that a three-component buffer system was sufficient to produce a virtually identical fit to the data for β_{total}.

$$\beta_{total}(pH) = \sum_{i=1}^{3} \frac{\ln(10) \times C_i \times 10^{pH-pK_i}}{\left(1 + 10^{pH-pK_i}\right)^2} \qquad (3)$$

Table 1 lists the parameters used to map the pH_i dependence of β_{total} in rat and guinea-pig myocytes. It is important to realize that eqn (3) is merely an empirical description of the data, permitting them to be coded into the model.

The algorithm for generating the LUTs deliberately excludes any assumption about the division of buffering into mobile and fixed components. Thus a given pH_i gradient is equated with an apparent intracellular buffer diffusion coefficient, lumped for a particular value of pH_i. On such a model, this coefficient equals the apparent diffusion coefficient for protons (D_H^{app}). All other factors being equal, significant variation in the size of the longitudinal gradient with pH_i indicates a pH_i sensitivity of D_H^{app}. The problem is that, if there is really a pH_i dependence, D_H^{app} will vary spatially along a longitudinal pH_i gradient. One way of assessing D_H^{app} would then be to estimate it over a range of end-to-end pH_i gradients, spread over a range of ambient pH_i values, each gradient with its own average pH_i. Experimentally, this would provide a statistical method of averaging the pH_i dependence of D_H^{app}. This is the approach adopted in the present work.

To reduce spatial variation of D_H^{app}, we partially perfused only low concentrations of NH_4Cl (3–5 mM). These usually restricted the size of the longitudinal pH_i gradient to 0.1–0.3 pH units, although larger gradients were still evident (up to 0.6 units) when pre-existing pH_i was low (see, e.g. Fig. 3*A*).

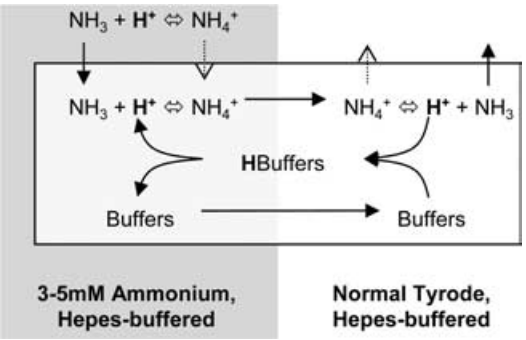

Figure 1. Schematic diagram of dual microperfusion: the computational model
Sarcolemmal and intracellular fluxes of solutes, as well as reaction events, are illustrated during partial exposure of a myocyte to small doses of NH_4Cl (3–5 mM). The result is an end-to-end pH_i gradient, as intracellular protonation of ammonia raises pH_i locally (by 0.1–0.6 pH units). Note that, because of buffering, the spatial diffusion of free H^+ is insignificant, all proton movement being via buffers (e.g. Vaughan-Jones *et al.* 2006). Sarcolemmal acid/base transporters are not included in the model, but it appears their effect on the pH_i gradient is negligible (Swietach *et al.* 2005*a*). The computational model is used to generate look-up-tables for apparent intracellular proton diffusion coefficient (D_H^{app}) as a function of the amplitude of the pH_i gradient for a given mean pH_i (see Methods).

Pipette dye-loading experiments

To measure the intracellular diffusion coefficient of carboxy-SNARF-1, guinea-pig cells were loaded with unesterified dye through patch-pipettes made from borosilicate capillary tubing (Harvard Apparatus, Edenbridge, UK; typical resistance, when filled, of 1–2 MΩ). Depending on the desired pH_i, cells were continuously superfused with normal Tyrode solution (for resting pH_i) or switched to superfusates containing 15 mM TMA (to induce a relatively stable alkalosis) or 80 mM acetate plus 30 μM cariporide (to induce a stable acidosis). After allowing 60 s for the stabilization of whole-cell pH_i, confocal emission fluorescence (at 580 and 640 nm) and transmission images were recorded every 2.1 s before and

after pipette break-in (see Fig. 4*B* and *C*). To monitor the progress of pipette attachment to the cell, the voltage was monitored using an Axoclamp 2B amplifier in 'Bridge' mode (Axon Instruments, Union City, CA, USA). Once the pipette had gained access to the cytoplasm following gentle suction, the dye was allowed to diffuse into the cell (for further details, see Vaughan-Jones *et al.* 2002 and Zaniboni *et al.* 2003). The progress of dye loading was measured as the rise in 580 or 640 nm emitted fluorescence averaged within three square ($10\,\mu m \times 10\,\mu m$) ROIs positioned downstream from the site of pipette attachment (see Fig. 4*Aa*). The time courses for dye loading were fitted with diffusion equations solved using the finite element method (Swietach *et al.* 2003; Zaniboni *et al.* 2003). The fits are usually very good for up to 120 s of dye loading, suggesting that the dye does not undergo significant binding, degradation or leakage from the cell. The ratio of carboxy-SNARF-1 fluorescence (at 580/640 nm) was used to estimate the pH_i at which dye loading was performed.

Statistics

Results are presented as means ± S.E.M. Two-tailed unpaired Student *t* tests at 5% significance level were used to test the significance between two populations. Multiple factor analysis of variation was performed at the 5% significance level. Correlation was quantified using Pearson's correlation coefficient. Best-fitting of data to user-defined functions was performed using MATLAB (Mathworks, USA).

Results

pH_i dependence of apparent proton mobility

Isolated rat and guinea-pig ventricular myocytes, AM-loaded with carboxy-SNARF-1, were imaged confocally for pH_i in three ROIs located at the ends and in the middle of the cell (Fig. 2*Aa* and *Ba*). Figure 2*Ab* shows pH_i time courses and spatial images of cellular pH_i recorded from a rat myocyte before and after an 8 min whole-cell prepulse with 30 mM ammonium. Prepulsing the cell induced a whole-cell acidosis of about 0.4 pH units. In all three ROIs, pH_i then started to recover slowly towards control levels as acid was extruded on sarcolemmal NHE. During this recovery period, the cell was partially exposed several times to 3 mM ammonium chloride delivered by switching on the dual microperfusion apparatus. Each partial exposure induced a longitudinal pH_i gradient of about 0.25 pH units, as illustrated in the specimen cellular images and in the time-course traces (Fig. 2*Ab*). Note that there was a tendency for the size of the gradient to decrease as whole-cell pH_i recovered.

Figure 2*Bb* shows cellular images and time courses of pH_i in three ROIs acquired from a guinea-pig myocyte (shown in Fig. 2*Bi*). The cell was subjected to a whole-cell prepulse with 80 mM acetate (8 min; Hepes-buffered superfusate). Upon acetate removal, a whole-cell alkalosis was induced, followed by a slow pH_i recovery as base was extruded via sarcolemmal Cl^-–OH^- exchange (Leem *et al.* 1999). During this recovery period, the dual microstream was switched on several times, partially exposing the cell to 3 mM ammonium. Each exposure induced a longitudinal pH_i gradient of around 0.15 units. There was a tendency for the amplitude of the gradient to increase as whole-cell pH_i recovered from the imposed alkalosis.

In total, 85 guinea-pig myocytes were partially perfused with ammonium (64 myocytes with 3 mM ammonium; 21 with 5 mM ammonium), and 138 rat cells were partially perfused with 3 mM ammonium. The end-to-end pH_i gradients measured during partial perfusion in these three populations were binned and plotted in Fig. 3*A* as a function of cell-averaged pH_i during dual microperfusion. A wide range of cell-averaged pH_i was encompassed, from 6.5 to 7.9. The purpose of using two doses of ammonium (in experiments with guinea-pig myocytes) was to investigate if there were any effects of concentration on the pH_i gradient mediated by factors other than the increase in the inward driving force for NH_3 (Swietach *et al.* 2005*a*). As shown later in Results, analysis of variation indicated no significant effect of ammonium concentration on the estimate of intracellular buffer mobility (D_{mob}). One in five experiments included cariporide in both microstreams to inhibit acid extrusion on NHE. Drug-containing superfusions coincided mainly with experiments in the more acidic range of pH_i, where strong activation of NHE would normally have occurred. Analysis of variation indicated that, for a given whole-cell pH_i, there was no significant difference between pH_i gradients observed in drug-free and drug-containing experiments ($P > 0.05$), as also reported previously (Swietach *et al.* 2005*a*). Therefore, drug-containing and drug-free data were combined.

Although the data shown in Fig. 3*A* were not corrected for variation in cell size and the longitudinal positioning of the dual microstream boundary, the trend in both rat and guinea-pig suggests a significant increase in longitudinal pH_i gradient size with a fall of pH_i. The raw data of Fig. 3*A* were converted to D_H^{app} using LUTs, as described in Methods. Values for D_H^{app} in rat and guinea-pig myocytes were binned and plotted in Fig. 3*B* as a function of cell-averaged pH_i. There was roughly a fivefold increase in D_H^{app} as pH_i rose from about 6.5 to 7.5 in both species ($P < 0.05$). According to the buffer hypothesis of proton mobility (eqn (1)), the variation of D_H^{app} may be caused by a pH_i-dependent change in the proportion of intracellular mobile-to-total buffering capacity (ϕ), or by a change in D_{mob}. Experiments were therefore designed to test both of these possibilities.

pH_i sensitivity of dye mobility

Fluorescent dyes have been used to study intracellular diffusion phenomena in heart (e.g. Imanaga *et al.* 1987; Vaughan-Jones *et al.* 2002). Several features make fluorophores useful as experimental models for simulating the movement of intrinsic mobile buffer: (i) they give a fluorescence signal proportional to concentration, which can be measured confocally with high spatiotemporal resolution; (ii) their molecular mass (and hence mobility) is similar to that predicted for mobile buffers (for example, the molecular mass for carboxy-SNARF-1 is 453 Da while, on average, it is estimated to be 190 Da for intrinsic mobile buffers; Vaughan-Jones *et al.* 2002); (iii) the fluorophore carboxy-SNARF-1 does not appear to undergo major degradation, binding or membrane transport inside the myocyte, and so its diffusion equation is simple in formulation (Zaniboni *et al.* 2003); and (iv) carboxy-SNARF-1 is, itself, a mobile buffer with a principal pK (~7.6) comparable to that predicted for several of the intrinsic mobile buffers (Vaughan-Jones *et al.* 2002), although its intracellular concentration in pH-imaging experiments is too low to influence physiological H_i^+ mobility. Any pH_i sensitivity in D_{mob} may therefore also be reflected in a similar pH_i sensitivity of the diffusion constant for carboxy-SNARF-1 (D_{SNARF}).

Figure 4*Aa* illustrates a dye-filled patch-pipette sealed onto a guinea-pig ventricular myocyte. Figure 4*Ab* and *Ac* shows the fluorescence signal measured during dye

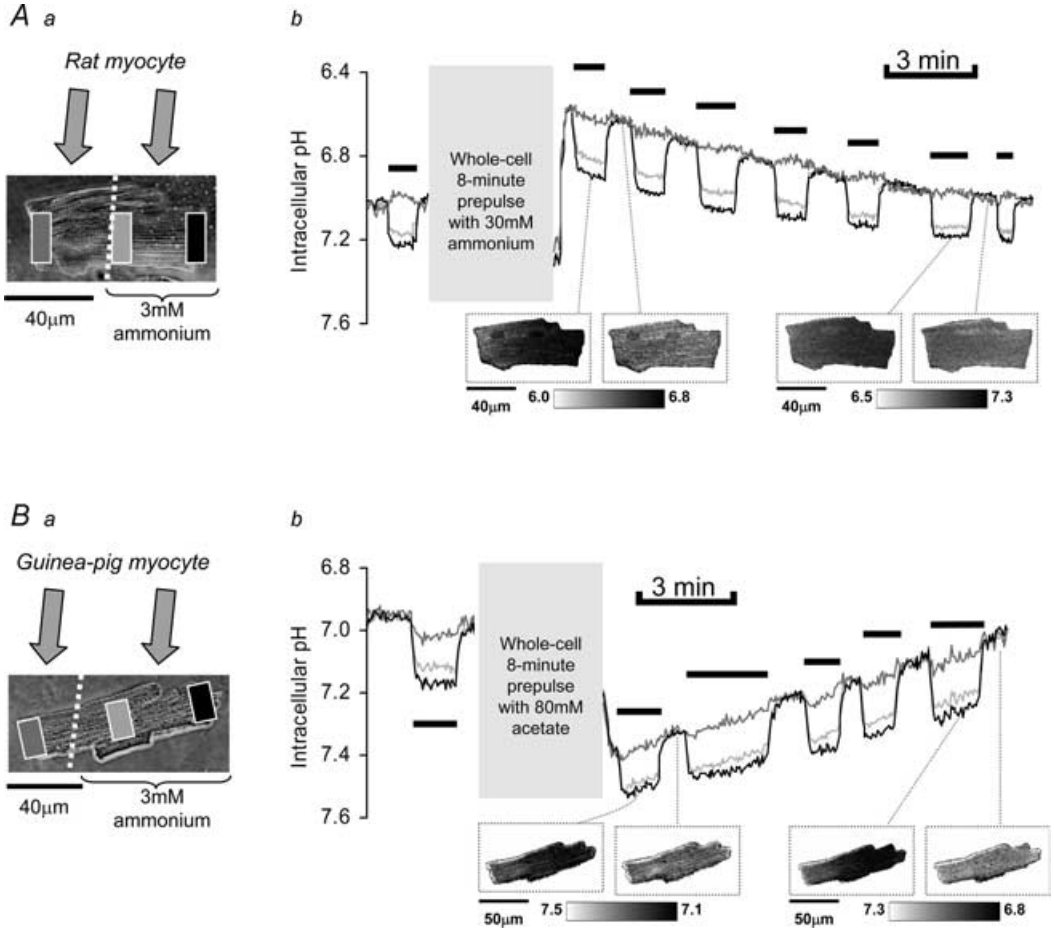

Figure 2. Experimental protocol for determining D_H^{app}
Aa, rat myocyte, illustrating regions of interest (ROIs), the position of the microstream boundary and the direction of microstream flow. *Ab*, pH_i time courses measured in the three ROIs before and after whole-cell superfusion with 30 mM ammonium (Hepes-buffered conditions). Horizontal bars indicate when partial perfusion with 3 mM ammonium was switched on. Inset, calibrated ratiometric cell images showing the regional pH_i during and after dual microperfusion at acid and normal pH_i. *Ba*, guinea-pig myocyte showing ROIs, the position of the microstream boundary and the direction of microstream flow. *Bb*, pH_i time courses measured in the three ROIs before and after whole-cell superfusion with 80 mM acetate (Hepes-buffered conditions). Horizontal bars indicate when partial perfusion with 3 mM ammonium was switched on. Inset, calibrated ratiometric cell images showing the regional pH_i during and after dual microperfusion at alkaline and normal pH_i. None of the solutions contained inhibitors of membrane acid/base transport. A model-fit to the time course for pH_i changes is shown in Fig. 7.

loading at 580 and 640 nm emission in three strategically located ROIs. It is possible to simulate the dye-loading time courses (Fig. 4*Ab* and *Ac*, grey lines) using the simple finite element diffusion algorithm (Zaniboni *et al.* 2003) run for a best-fitting value of dye diffusion coefficient (D_{SNARF}). This and similar experiments were performed at resting pH$_i$, maintained by normal Tyrode superfusion. Other experiments were performed during cell superfusion with 15 mM TMA to raise whole-cell pH$_i$ for 4 min (as illustrated in Fig. 4*C*), or 80 mM acetate plus 30 μM cariporide to reduce pH$_i$ tonically (as illustrated in Fig. 4*B*). The grey arrows in Fig. 4*B* and *C* indicate the moment when dye loading would normally commence. The relative constancy of pH$_i$ during the prepulse is a condition necessary for ensuring that the change in fluorescence during dye loading is purely due to the spread of dye, rather than a result of pH$_i$ changes.

Figure 4*D* shows binned data for D_{SNARF}, plotted *versus* the cell-averaged pH$_i$. The black and grey symbols refer to dye fluorescence measured at 580 and 640 nm, respectively. At the different pH$_i$ levels tested, D_{SNARF} was not significantly different (t test, $P \gg 0.05$, correlation coefficient $r^2 = 0.00195$), suggesting that D_{SNARF} is pH$_i$ insensitive over the physiological pH$_i$ range. The average D_{SNARF} was $1.47\,(\pm 0.12) \times 10^{-7}$ cm^2 s^{-1} when measured at 580 nm, and $1.44\,(\pm 0.12) \times 10^{-7}$ cm^2 s^{-1} when measured at 640 nm (these measurements should be interpreted assuming the two forms interconvert via rapid protonation). Pooled data suggest a D_{SNARF} of $1.46\,(\pm 0.12) \times 10^{-7}$ cm^2 s^{-1}. This is similar to results reported by Vaughan-Jones *et al.* (2002) in rabbit myocytes (0.9×10^{-7} cm^2 s^{-1}) and Zaniboni *et al.* (2003) in guinea-pig myocytes ($3.22\,(\pm 0.86) \times 10^{-7}$ cm^2 s^{-1}). Taking these results as a model for intrinsic mobile buffer, they suggest that D_{mob} may also show no significant pH$_i$ dependence, at least in the physiological range. The mobility of intracellular carboxy-SNARF-1 is considered further in the Discussion.

Capacity of mobile buffer and its diffusion coefficient

As mentioned above, the considerable pH$_i$ sensitivity of D_H^{app} shown in Fig. 3*B* is likely to be caused by a significant difference in the pH$_i$ dependence of mobile and fixed buffering capacity rather than by changes in D_{mob}. The data of Fig. 3*B* can be deconvoluted into a measure of β_{mob} and β_{fix}, if it is assumed that fixed buffering is principally due to residues with pK values clustered around a single value, as suggested by Zaniboni *et al.* (2003),

$$\beta_{fix} = \frac{\ln(10) \times C_{fix} \times 10^{pH_i - pK_{fix}}}{\left(1 + 10^{pH_i - pK_{fix}}\right)^2} \quad (4)$$

where C_{fix} is the concentration, and pK_{fix} is the pH for maximal fixed buffering capacity. Since the previous section suggested that D_{mob} may be pH$_i$ independent, eqn (4) and eqn (2) can be substituted into eqn (1) to give the following:

$$D_H^{app} = D_{mob} \frac{\beta_{total}(pH_i) - \dfrac{\ln(10) \times C_{fix} \times 10^{pH_i - pK_{fix}}}{(1 + 10^{pH_i - pK_{fix}})^2}}{\beta_{total}(pH_i)} \quad (5)$$

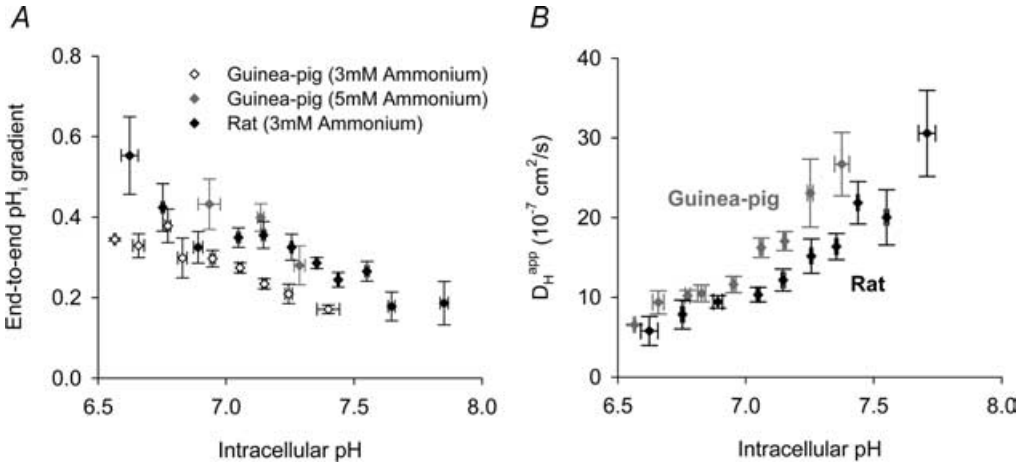

Figure 3. Size of end-to-end pH$_i$ gradient, and the apparent proton diffusion coefficient
A, data were pooled into three categories: guinea-pig myocytes exposed to 3 mM ammonium (open symbols, from left to right: $n = 3,3,7,5,13,12,13,5,3$) and 5 mM ammonium (grey symbols, $n = 4,11,6$), and rat myocytes exposed to 3 mM ammonium (black symbols, $n = 5,9,7,16,18,13,24,21,15,10$). Mean cell length: 125.4 ± 2.7 μm (guinea-pig, $n = 64$), 107.2 ± 1.3 μm (rat, $n = 53$); mean cell width: 26.8 ± 0.6 μm (guinea-pig), 25.4 ± 0.6 μm (rat); mean cellular exposure to ammonium during dual microperfusion: 50.2 ± 1.3% (guinea-pig), 44.4 ± 0.8% (rat). *B*, data for D_H^{app} derived from dual microperfusion experiments performed on isolated guinea-pig myocytes (grey symbols; $n = 3,3,7,6,16,15,21,9,5$) and rat myocytes (black symbols; $n = 5,9,7,16,18,13,24,21,15,10$).

The relationship between β_{total} and pH_i has been determined previously by Zaniboni *et al.* (2003; diamond symbols and light grey curve in Fig. 5) and is described empirically by eqn (3) (see Methods). Since the relationship between D_H^{app} and pH_i has been determined independently in the present work (Fig. 3*B*), this leaves three unknown parameters in eqn (5): pK_{fix}, C_{fix} and D_{mob}. These constants were estimated by using eqn (5) to best-fit the relationship between D_H^{app} and pH_i shown in Fig. 3*B* (done using the least-squares method). Table 2 summarizes the results. By rearranging eqn (1), β_{mob} can be expressed in terms of the mobile buffer's diffusion coefficient (D_{mob}, see Table 2), β_{total}, and D_H^{app} (Fig. 3*B*) as follows:

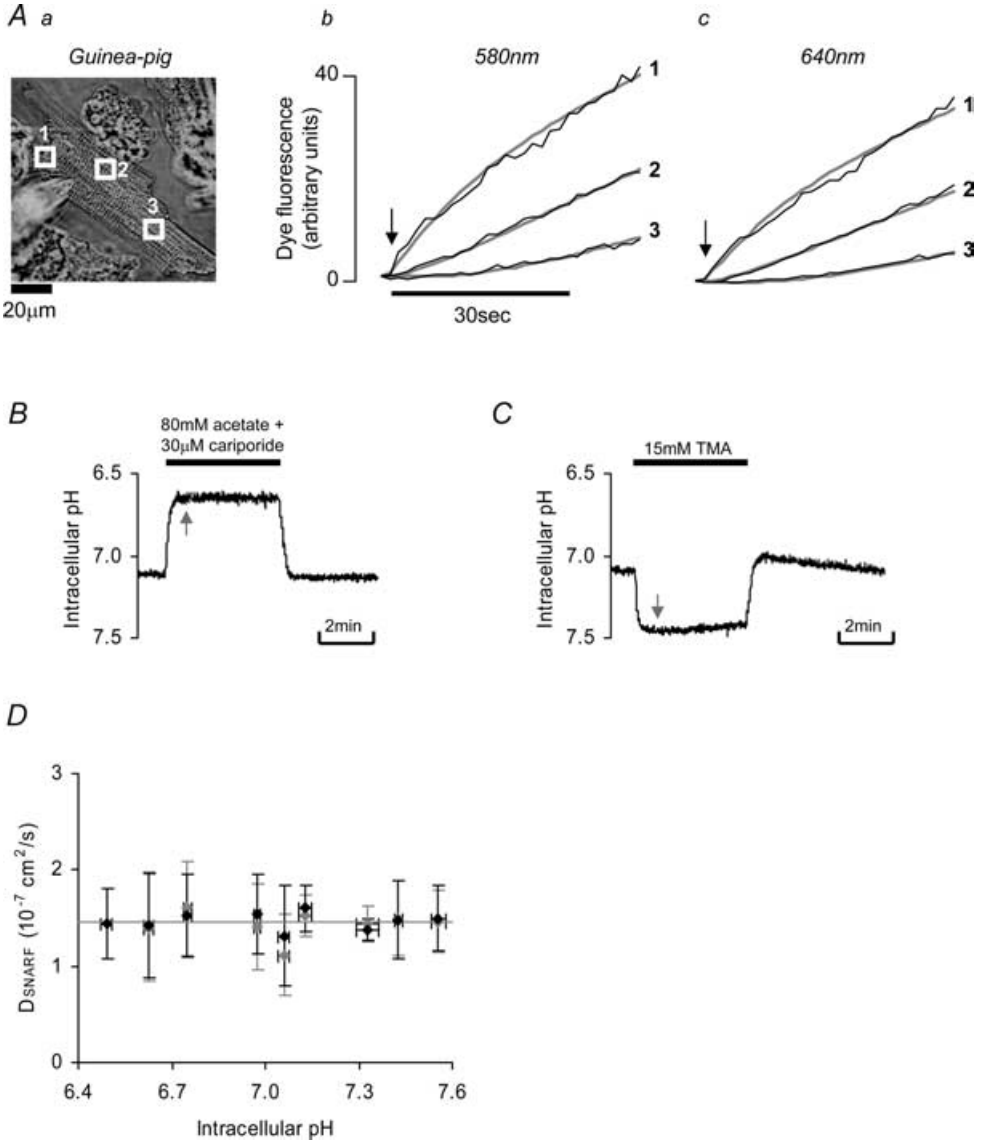

Figure 4. Effect of changing pH_i on intracellular carboxy-SNARF-1 mobility
Aa, guinea-pig myocyte showing the position of three ROIs and the pipette. The time courses of dye loading in the three ROIs were measured at 580 and 640 nm, as shown in *Ab* and *Ac*. Units on the vertical axis are arbitrary, but proportional to concentration. *B*, whole-cell pH_i time course measured during a 4 min prepulse with 80 mM acetate (with 30 μM cariporide), showing a stable acidosis under Hepes-buffered conditions. *C*, whole-cell pH_i time course measured during a 4 min prepulse with 15 mM trimethylamine (TMA), showing a stable alkalosis under Hepes-buffered conditions. The grey arrows point to the start of a typical dye-loading experiment, coinciding with a stable pH_i level. *D*, binned data from experiments performed at acidic, resting and alkaline pH_i ($n = 5,4,5,5,4,5,4,6,3$). Mean pH_i was calculated from the ratio of 580 nm to 640 nm fluorescence. Black symbols refer to estimates of carboxy-SNARF-1 diffusion coefficient (D_{SNARF}) calculated from 580 nm fluorescence data. Grey symbols refer to estimates of D_{SNARF} from 640 nm fluorescence. The straight line shows the mean D_{SNARF}.

$$\beta_{mob} = \frac{D_H^{app}}{D_{mob}}\beta_{total} \quad (6)$$

Using eqn (6), one may then derive the pH$_i$ dependence of β_{mob} in rat and guinea-pig myocytes (filled circles in Fig. 5*A* and *B*).

To simplify the characterization of β_{mob}, it was assumed to comprise a single population of concentration C_{mob}, and a pH at optimum buffering capacity of pK_{mob}. Table 2 summarizes the results of the least-squares fitting of the relationship between β_{mob} and pH$_i$. Figure 5 shows the pooled, single component for mobile buffer (β_{mob}, black curve) and fixed buffer (β_{fix}, dark grey curve), as well as the fit previously described for β_{total} (Zaniboni *et al.* 2003; light-grey curve). This analysis therefore divides total buffering capacity simplistically into fixed and mobile populations of buffer (see Table 2 for values of these parameters) where:

$$\beta_{total} = \frac{\ln(10) \times C_{mob} \times 10^{pH-pK_{mob}}}{(1+10^{pH-pK_{mob}})^2} + \frac{\ln(10) \times C_{fix} \times 10^{pH-pK_{fix}}}{(1+10^{pH-pK_{fix}})^2} \quad (7)$$

Figure 5*A* and *B* shows that, over the pH$_i$ range 6.5–7.5, the sum of values deduced for mobile and fixed buffering capacity ($\beta_{mob} + \beta_{fix}$) is in close agreement with the empirical description of β_{total} measured previously (Zaniboni *et al.* 2003). Outside this pH$_i$ range, however, the agreement is less precise, possibly because mobile and/or fixed buffering can no longer be considered as unimodal. It is, for example, possible that mobile buffering capacity increases below pH$_i$ 6.5 due to additional contributions from buffers with lower pK values, such as MgATP and phosphocreatine (Vaughan-Jones *et al.* 2002).

Table 2. Characteristics of intracellular fixed and mobile buffer results for guinea-pig and rat ventricular myocytes of least-squares fitting of data in Fig. 3*B*, using eqn (5)

Fitting parameter	Units	Guinea-pig	Rat
C_{fix}	mM	67.1 (±6.0)	62.4 (±1.2)
pK_{fix}	dimensionless	6.29 (±0.11)	6.40 (±0.13)
D_{mob}	10^{-7} cm^2 s^{-1}	64.8 (±16.8)	49.9 (±11.4)
C_{mob}	mM	12.5 (±1.4)	13.7 (±1.9)
pK_{mob}	dimensionless	7.30 (±0.14)	7.48 (±0.18)

Parameter values are followed (in parentheses) by their 95% confidence interval.

The constants in Table 2, when substituted into eqn (1), can be used to predict the mobile-to-total buffering capacity ratio, and hence D_H^{app} as a function of pH$_i$. This has been plotted (continuous lines) in Fig. 6 for both guinea-pig and rat myocytes. Superimposed on these lines are experimental estimates of D_H^{app} determined over a range of pH$_i$ values. The predictions fit the data remarkably well.

The ability of the diffusion–reaction model to predict experimental results was then tested by simulating the regional pH$_i$ time courses measured in the experiments illustrated in Fig. 2, again using values deduced (Table 2) for fixed and mobile buffer. The good correspondence of model simulation (Fig. 7, black trace) and experimental result (Fig. 7, grey trace) in rat and guinea-pig cells is strong evidence in favour of the pH$_i$ dependence of H_i^+ mobility plotted in Fig. 6. For the simulations presented in Fig. 7,

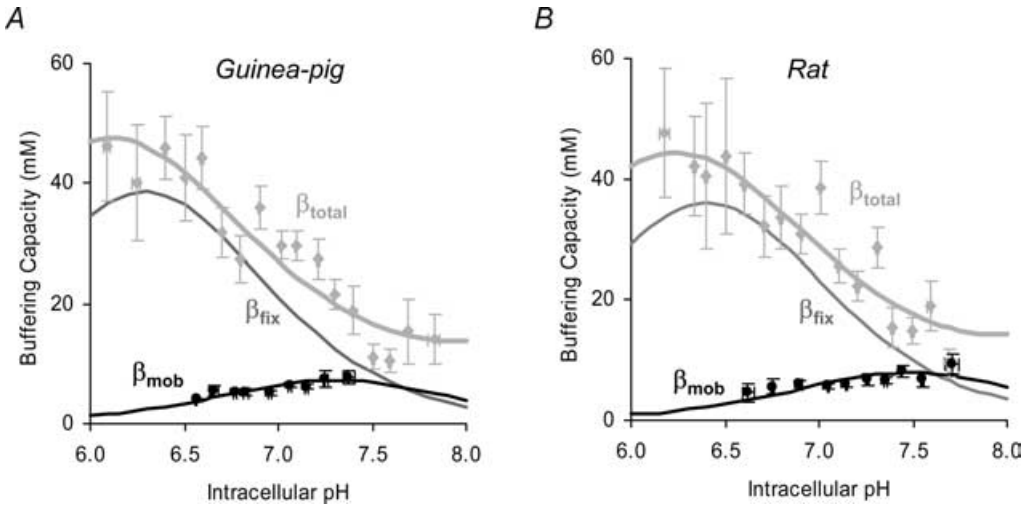

Figure 5. Mobile and fixed components of intrinsic buffering
Results for guinea-pig (*A*) and rat (*B*) myocytes showing data for total intrinsic buffer capacity (light grey symbols and curve, from Zaniboni *et al.* 2003) and mobile buffering capacity (black symbols, derived from Fig 3*B* and Eqn 6). The black curve describes a one-component (single pK_{mob}) best-fit to data for mobile buffering (Table 2). Similarly, the dark grey curve describes a one-component (single pK_{fix}) fixed buffering capacity relationship, based on the parameters in Table 2.

sarcolemmal acid/base flux on rat Na^+–H^+ exchange or guinea-pig Cl^-–OH^- exchange (CHE) was also included in the model, using equations derived from whole-cell pH_i recovery time courses, as determined previously (Leem *et al.* 1999; Swietach *et al.* 2005*a*):

$$J^{\mathrm{NHE}} = 10.5\frac{[\mathrm{H}^+]^{1.933}}{[\mathrm{H}^+]^{1.933} + (10^{6.38})^{1.933}}$$

$$J^{\mathrm{CHE}} = 68.988\left(\exp\left(\frac{[\mathrm{H}^+]}{0.01781}\right) - 1\right)$$

where J^{NHE} is acid efflux on NHE in mM min^{-1}, and J^{CHE} is base efflux on CHE in M min^{-1}. Having estimated the mobile-to-total buffering capacity ratio, it is possible to convert $D_{\mathrm{H}}^{\mathrm{app}}$ into an estimate of D_{mob} for each experiment, using eqn (1). D_{mob} should be independent of pH_i (cf. the carboxy-SNARF-1 diffusion experiments), and independent of the presence of cariporide, of cell-length and of the concentration and the extent of partial exposure to ammonium. This hypothesis was tested by multiple factor analysis of variation, which showed no significant difference ($P > 0.05$) when D_{mob} was grouped according to any of the parameters listed above. This strengthened the argument that the mechanism underlying the pH_i dependence of $D_{\mathrm{H}}^{\mathrm{app}}$ is the pH_i sensitivity of the mobile-to-total buffering capacity.

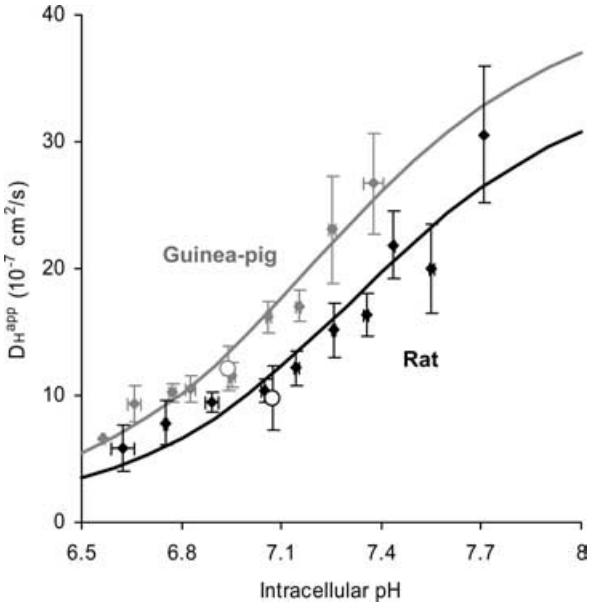

Figure 6. pH_i dependence of proton mobility
The curves show the predicted relationship between $D_{\mathrm{H}}^{\mathrm{app}}$ and intracellular pH using the mobile and fixed buffering capacities and mobile buffer diffusion coefficient listed in Table 2. Superimposed on the curves are data from Fig. 5 (filled symbols) and data (open symbols) from Zaniboni *et al.* (2003). The grey curve and data points refer to guinea-pig myocytes; the black curve and data points refer to rat myocytes. The Zaniboni *et al.* data for $D_{\mathrm{H}}^{\mathrm{app}}$ were derived from pipette acid-loading experiments, and have been plotted *versus* cell-averaged pH_i after 30 s of acid loading ($n = 20$ for guinea-pig and $n = 11$ for rat).

Discussion

Intracellular proton mobility is pH_i sensitive

The present work confirms that intracellular H^+ mobility in ventricular myocytes is much lower than in unbuffered solution. More importantly, it provides the first experimental evidence that, in guinea-pig and rat ventricular myocytes, intracellular proton mobility is not constant, but varies with pH_i. There is a fivefold increase of $D_{\mathrm{H}}^{\mathrm{app}}$ as pH_i is raised from 6.5 to 7.5. The most likely explanation for the increase is that, over this pH_i range, intrinsic mobile buffering capacity increases, while fixed buffering capacity decreases (see Fig. 5). The fraction of buffering that is available to shuttle protons therefore

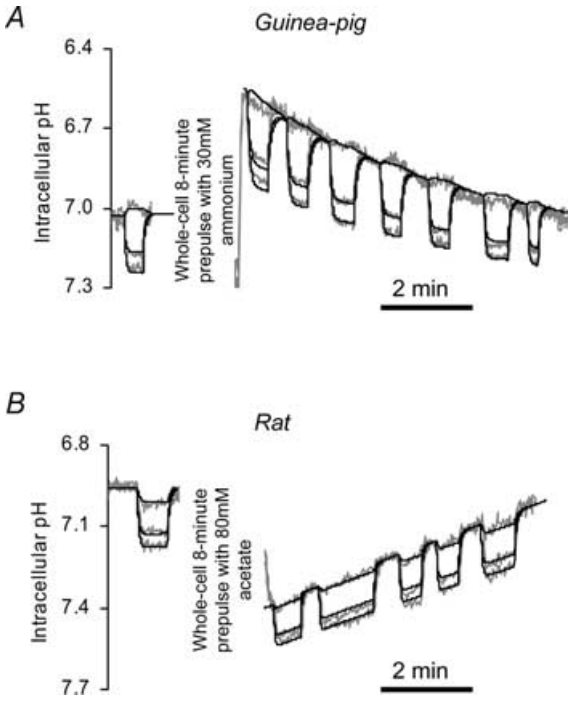

Figure 7. Computational simulation of dual microperfusion
Using data from Fig. 2, it was possible to run a two-buffer (fixed and mobile) diffusion–reaction simulation (using parameters listed in Table 2) together with a sarcolemmal H^+-transport mechanism to account for whole-cell pH_i recovery from acidosis (i.e. NHE) and alkalosis (i.e. CHE). The cell geometry and protocol applied in the simulation were identical to those in the experiment shown in Fig. 2. *A*, rat myocyte: time course of pH_i averaged in three ROIs (positioned along the cell as in Fig. 2*Aa*) during a series of partial exposures to NH_4Cl, before and after a whole-cell intracellular acid load (whole-cell 30 mM ammonium prepulse). *B*, guinea-pig myocyte: time course of pH_i averaged in three ROIs (positioned along the cell, as in Fig. 2*Ba*) during a series of partial exposures to NH_4Cl before and after a whole-cell intracellular alkaline load (whole-cell 80 mM acetate prepulse). The experimental data (grey) and model simulation (black) are in very good agreement.

increases greatly at alkaline pH$_i$, thus increasing H_i^+ mobility.

The possibility that an increase of D_{mob} at high pH$_i$ also enhances H_i^+ mobility cannot be ruled out, but our observations on the diffusion of intracellular carboxy-SNARF-1, itself a mobile buffer, suggest that this is unlikely. Carboxy-SNARF-1 is of moderate molecular mass (453 Da), and its fluorescence is affected by the binding of a single proton (pK ~7.6). Although its buffering capacity in the cell (<0.2 mM; Vaughan-Jones *et al.* 2002) is too low to affect proton mobility, its diffusive properties are likely to resemble those of the intrinsic mobile buffers. These latter buffers are believed to be mainly histidyl dipeptides, such as homocarnosine, acetyl anserine and acetyl carnosine (O'Dowd *et al.* 1988), which are present collectively in ventricular tissue at a concentration of about 17 mM, and which could provide a mobile buffering capacity (at pH$_i$ 7.1) of about 8 mM (for a list of intracellular mobile buffers, their concentration, and their capacity in the cardiac cell, see Table 1 of Vaughan-Jones *et al.* 2002). If, for example, the protonated form of intracellular carboxy-SNARF-1 were to display a lower diffusion coefficient than the unprotonated form, overall dye diffusion would be slower at a low pH (when the protonated form is dominant, given a rapid interconversion between both forms). The fact that the apparent value of D_{SNARF} (i.e. the value lumped for both diffusive forms) is similar at high and low pH$_i$ suggests that both forms have similar diffusion constants. The standard error of the gradient of the regression line to the data shown in Fig. 4*D* indicates that, at most, the intracellular diffusion coefficient for the two forms of dye should differ by no more than 14% (details of this calculation are presented in the online supplement). By extrapolation, it is therefore likely that the protonated and unprotonated forms of intrinsic mobile buffer also diffuse at comparable rates, i.e. D_{mob} is pH$_i$ insensitive.

The above conclusion points to the ratio of mobile-to-total buffering capacity as the prime determinant of the pH$_i$ sensitivity of H_i^+ mobility. By using simple buffering equations in combination with our pH$_i$ imaging data, we have obtained the first experimental estimate in an intact cell of the mobile and fixed components of intrinsic buffering capacity (Fig. 5), and the mobile buffer diffusion coefficient (Table 2). The estimates of β_{mob} and β_{fix} are similar to recent predictions based on the possible chemical composition of intrinsic mobile and fixed buffers (Zaniboni *et al.* 2003; β_{fix} was assumed largely to reflect imidazole residues on cytoplasmic proteins). The estimates of β_{mob} and β_{fix} also resemble the dual-buffer system proposed by Leem *et al.* (1999) for the myocyte's intrinsic buffering capacity. The buffer characteristics accurately predict the experimentally determined pH$_i$ dependence of D_H^{app} (Fig. 6). Furthermore, the values of D_H^{app} measured in the present work are in good agreement with previous experimental estimates obtained using local pipette loading of acid rather than dual microperfusion (Zaniboni *et al.* 2003; and shown as open symbols in Fig. 6). Lastly, when using the experimentally determined values for fixed and mobile buffer capacity and mobility, our diffusion–reaction model is able to predict the spatiotemporal behaviour of intracellular pH with a remarkably high degree of accuracy, as illustrated in Fig. 7. This all provides strong supporting evidence for the buffer hypothesis of H_i^+ mobility.

A pH$_i$-dependent increase of mobile buffering capacity was proposed to account for the threefold increase of H^+ mobility in axoplasm extracted from the marine invertebrate *Myxicola* following a rise of pH from about 6.6 to >8.2 (Al-Baldawi & Abercrombie, 1992). In that case, mobile buffering was attributed to the high cytoplasmic concentrations of the amino acids glycine, L-cysteic acid and aspartic acid (with a combined concentration of 374 mM). Amino acid concentrations in mammalian myocardial tissue are much lower (with a combined concentration of about 11 mM; Vaughan-Jones *et al.* 2002) and their pK values ensure that they contribute little to physiological buffering and hence to H_i^+ mobility. Intracellular taurine is present at about 30 mM in heart, but with a pK value close to 9.0, this solute would only become a significant mobile buffer at pH$_i$ values >8.5.

Intracellular diffusion coefficients have previously been measured for a variety of unbuffered solutes in myoplasm. Figure 8 plots the empirical relationship

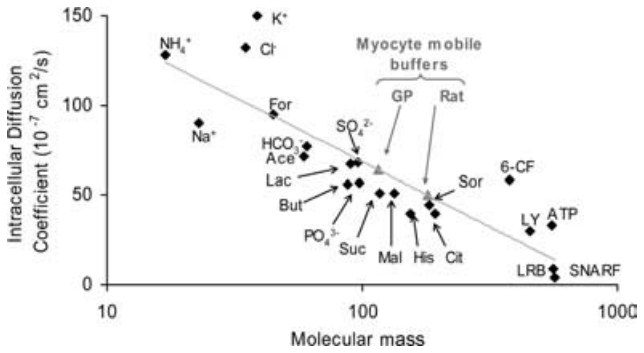

Figure 8. Empirical relationship between molecular mass of a solute and its intracellular diffusion coefficient in muscle cells
Data were obtained from Kushmerick & Podolsky (1969) for K^+, Na^+, sulphate, phosphate, sorbitol (Sor) and ATP; Imanaga *et al.* (1987) for lissamine rhodamine B-200 (LRB), Lucifer yellow (LY) and 6-carboxyfluorescein (6-CF); Swietach *et al.* (2003) for NH_4^+, HCO_3^-, acetate (Ace), butyrate (But), citrate (Cit), Cl^-, formate (For), histidine (His), lactate (Lat), malate (Mal), succinate (Suc). The mobile buffer (grey symbols) and carboxy-SNARF-1 (SNARF) data were obtained from Table 2 and Fig. 4*D*, respectively. Data were measured at, or corrected to, a temperature of 37°C. The grey line shows the empirical relationship described by eqn (8). This relationship was used to assign a mean molecular mass to mobile buffers within the mammalian cardiomyocyte.

between molecular mass and diffusion coefficient (D) compiled from Kushmerick & Podolsky (1969), Imanaga *et al.* (1987), Swietach *et al.* (2003) and Zaniboni *et al.* (2003). For the Kushmerick & Podolsky data, a correction factor was applied to allow for the temperature dependence of diffusion (temperature coefficient (Q_{10}) ~1.5), as their experiments were performed at room temperature. Superimposed on the data is the best-fitting line (plotted on a logarithmic scale):

$$D = -31.54 \ln(\text{molecular mass}) + 213.65 \qquad (8)$$

This fitting equation was used to assign a population-averaged molecular mass to intracellular mobile buffers, based on their mobility (D_{mob} from Table 2). The mean mobile buffer molecular mass was found to be 112 Da (95% confidence interval, 66–191 Da) and 180 Da (95% confidence interval, 125–258 Da) for guinea-pig and rat myocytes, respectively. These values match the mean molecular mass (~190 Da) of mobile buffers predicted by Vaughan-Jones *et al.* (2002). Although the value of D_{mob} determined in guinea-pig and rat myocytes is not significantly different, a lower mobility in rat myoplasm may be explained by the relatively larger degree of membrane infolding, thus imposing a greater hindrance to diffusion (see Table 1).

As pointed out earlier, the typical H_i^+ mobility estimated in the present work (5×10^{-7} to 2.5×10^{-6} cm^2 s^{-1}, depending on the value of pH_i) is much lower than the H^+ diffusion coefficient measured in pure water (~10^{-4} cm^2 s^{-1}, Vanysek, 1999). Due to reaction processes with buffers, the diffusion coefficient for intracellular protons will *not* fit the empirical relationship of eqn (8). Likewise, intracellular Ca^{2+} buffering reduces the diffusion coefficient for Ca^{2+} ions by two orders of magnitude, to 3×10^{-6} cm^2 s^{-1} (Baylor & Hollingworth, 1998; Cordeiro *et al.* 2001) or even to ~2×10^{-7} cm^2 s^{-1} (Gabso *et al.* 1997).

Physiological relevance of pH-sensitive H_i^+ mobility

The pH_i sensitivity of H_i^+ mobility is governed by the characteristics of the mobile and fixed intracellular buffers. Intrinsic buffering power is relatively high in cardiac cells (15–50 mM, depending on pH_i, see Fig. 5). Such a high capacity is required to prevent cytoplasmic proteins from being exposed to large and rapid fluctuations of pH. Perhaps because of cellular economy, most buffering occurs on the proteins themselves.

Proteins cannot be the sole intracellular buffers as their low diffusibility would reduce D_H^{app} to unacceptably low levels, preventing sarcolemmal H^+ transporters from regulating bulk pH_i. There is thus a requirement for lower molecular mass, diffusible buffers to provide adequate proton mobility. Many of these compounds also serve other purposes as metabolic solutes, energy substrates, and osmolytes. Their concentration may therefore be constrained by factors other than their requirement for mobile buffering (e.g. metabolic, degradative or osmotic factors may be equally important), and this may contribute to their concentration being lower than that of protein buffers. Nevertheless, the modest level of intrinsic mobile buffer is usually sufficient to maintain adequate diffusive H^+-coupling between bulk cytoplasm and the sarcolemmal acid/base transporters. Under some circumstances, however, the low H_i^+ mobility imposed by buffers can result in significant local nonuniformity of pH_i. This can occur, for example, during high rates of activity of the pH regulatory transporter, NHE (Swietach & Vaughan-Jones, 2005), or during local sarcolemmal H^+ fluxes induced by extracellular gradients of membrane permeant weak acid or base such as CO_2 or ammonia (Spitzer *et al.* 2000; Swietach *et al.* 2005*a*). The latter process may be prevalent in clinical conditions such as regional myocardial ischaemia where there is local heterogeneity of partial pressure of CO_2 and where pH_i may be as low as 6.0 (Garlick *et al.* 1979). The diffusive properties of H^+ ions in ischaemic tissue have yet to be investigated, but the present work indicates that any tendency of normal myocardium to exhibit pH_i nonuniformity will be exacerbated during intracellular acidosis because of the simultaneous fall in H_i^+ mobility.

H_i^+ mobility in the presence of carbonic buffer

Although the present work was performed under nominally CO_2/HCO_3^--free conditions (using superfusates buffered with Hepes), a comparable pH_i dependence of D_H^{app} is likely to occur in the presence of extrinsic carbonic buffer. Intracellular CO_2/HCO_3^- acts as an additional mobile buffer that can enhance H_i^+ mobility (Stewart *et al.* 1999; Spitzer *et al.* 2002; Zaniboni *et al.* 2003). This influence, however, is largely confined to the more alkaline range of pH_i. For example, for a typical partial pressure of CO_2 of 40 mmHg (5% CO_2), intracellular carbonic buffering capacity at pH_i 7.4 is about 50 mM (Leem *et al.* 1999), but it declines exponentially with pH_i, being ~2 mM at pH_i 6.0. This reflects the dramatic fall of intracellular HCO_3^- concentration under these conditions. Spatial shuttling of intracellular protons on carbonic buffer is therefore likely to decline at low pH_i, in parallel with the decline on the intrinsic buffer shuttle.

Unfortunately, dual microperfusion cannot readily be used to explore the influence of CO_2/HCO_3^- on H_i^+ mobility. This is because local exposure to ammonia produces a large flux of acid down the cell, carried on intrinsic buffer, which overwhelms the slow equilibration between intracellular CO_2 and HCO_3^-, resulting in a much smaller acid flux carried on carbonic buffer (Swietach *et al.* 2005*a*). At high intracellular acid flux, the carbonic

flux therefore becomes difficult to resolve. We have recently used local photolytic uncaging of protons from intracellular NBA (2-nitrobenzaldehyde; loaded from the extracellular solution; cf. Schwiening, 2004) to explore H_i^+ mobility in the rat ventricular myocyte (Swietach *et al.* 2005*b*). This technique produces a much smaller acid flux within the cell, permitting one to assess the role of carbonic buffer. By locally uncaging intracellular protons while superfusing the cell with 5% CO_2/22 mM HCO_3^--buffered Tyrode solution, we have obtained preliminary evidence that reducing pH_i from 7.1 to 6.5 results in a decline of H_i^+ mobility, comparable to that reported in the present work in the absence of CO_2/HCO_3^- (P. Swietach & R. D. Vaughan-Jones, unpublished observations). Furthermore, although H_i^+ mobility appears to be enhanced by carbonic buffer at the higher pH_i (about twofold), in agreement with previous results using local acid injection from a micropipette (Zaniboni *et al.* 2003), no significant enhancement has been observed at pH_i 6.5, consistent with failure of the carbonic buffer shuttle at low $[HCO_3^-]_i$. It is therefore likely that the pH_i dependence of D_H^{app} will be preserved in the presence of CO_2/HCO_3^- buffer.

Conclusions

In conclusion, intrinsic mobile buffer is an essential component of the pH_i regulatory apparatus, serving to couple the cytoplasm spatially to H^+-equivalent transport reactions at the sarcolemma. At low pH_i, this spatial coupling will be weakened, because much of the intrinsic mobile buffer is occupied, while fixed buffering is enhanced. Under these conditions, a large intracellular acidosis combined with rapid acid flux within the cell or across the sarcolemma will predispose a myocyte to pH_i nonuniformity. Intracellular microdomains of differing pH, when they occur, are likely to reduce the efficient co-ordination of spatially distributed proteins within the cell (such as contractile proteins) that display strong pH sensitivity. The physiological regulation of H_i^+ mobility is thus a process fundamental to the functional activity of a cardiomyocyte.

References

Al-Baldawi NF & Abercrombie RF (1992). Cytoplasmic hydrogen ion diffusion coefficient. *Biophys J* **61**, 1470–1479.

Allen DG & Orchard CH (1983). The effects of changes in pH on intracellular calcium transients in mammalian cardiac muscle. *J Physiol* **335**, 555–567.

Baylor SM & Hollingworth S (1998). Model of sarcomeric Ca^{2+} movements, ATP Ca^{2+} binding and diffusion, during activation of frog skeletal muscle. *J Gen Physiol* **112**, 297–316.

Bountra C & Vaughan-Jones RD (1989). Effect of intracellular and extracellular pH on contraction in isolated, mammalian cardiac muscle. *J Physiol* **418**, 163–187.

Choi HS, Trafford AW, Orchard CH & Eisner DA (2000). The effect of acidosis on systolic Ca^{2+} and sarcoplasmic reticulum calcium content in isolated rat ventricular myocytes. *J Physiol* **529**, 661–668.

Cordeiro JM, Spitzer KW, Giles WR, Ershler PE, Cannell MB & Bridge JHB (2001). Location of the initiation site of calcium transients and sparks in rabbit heart Purkinje cells. *J Physiol* **531**, 301–314.

Eigen M (1964). Proton transfer, acid-base catalysis, and enzymatic hydrolysis. Part I: elementary processes. *Ang Chem Int Ed* **3**, 1–19.

Gabso M, Neher E & Spira ME (1997). Low mobility of the Ca^{2+} buffers in axons of cultured *Aplysia* neurons. *Neuron* **18**, 473–481.

Garlick PB, Radda GK & Seeley PJ (1979). Studies of acidosis in the ischaemic heart by phosphorus nuclear magnetic resonance. *Biochem J* **184**, 547–554.

Harrison SM, Frampton JE, McCall E, Boyett MR & Orchard CH (1992). Contraction and intracellular Ca^{2+}, Na^+ and H^+ during acidosis in rat ventricular myocytes. *Am J Physiol Cell Physiol* **262**, C348–357.

Imanaga I, Kameyama M & Irisawa H (1987). Cell-to-cell diffusion of fluorescent dyes in paired ventricular cells. *Am J Physiol Heart Circ Physiol* **252**, H223–232.

Irving M, Maylie J, Sizto NL & Chandler WK (1990). Intracellular diffusion in the presence of mobile buffers. Application to proton movement in muscle. *Biophys J* **57**, 717–721.

Junge W & McLaughlin S (1987). The role of fixed and mobile buffers in the kinetics of proton movement. *Biochim Biophys Acta* **890**, 1–5.

Kushmerick MJ & Podolsky RJ (1969). Ionic mobility in muscle cells. *Science* **166**, 1297–1298.

Lagadic-Gossmann D, Buckler KJ & Vaughan-Jones RD (1992). Role of bicarbonate in pH recovery from intracellular acidosis in the guinea-pig ventricular myocyte. *J Physiol* **458**, 361–384.

Leem CH, Lagadic-Gossmann D & Vaughan-Jones RD (1999). Characterization of intracellular pH regulation in the guinea-pig ventricular myocyte. *J Physiol* **517**, 159–180.

O'Dowd JJ, Robins DJ & Miller DJ (1988). Detection, characterisation and quantification of carnosine and other histidyl derivatives in cardiac and skeletal muscle. *Biochim Biophys Acta* **967**, 241–249.

Orchard CH & Kentish JC (1990). Effects of changes of pH on the contractile function of cardiac muscle. *Am J Physiol Cell Physiol* **258**, C967–981.

Satoh H, Delbridge LM, Blatter LA & Bers DM (1996). Surface:volume relationship in cardiac myocytes studied with confocal microscopy and membrane capacitance measurements: species-dependent and developmental effects. *Biophys J* **70**, 1494–1504.

Scholz W, Albus U, Counillon L, Gogelein H, Lang HJ, Linz W, Weichert A & Scholkens BA (1995). Protective effects of HOE642, a selective sodium-hydrogen exchange subtype 1 inhibitor, on cardiac ischaemia and reperfusion. *Cardiovasc Res* **29**, 260–268.

Schwiening CJ (2004). Rapid regionally restricted pH_i shifts in neurons induced by the photolysis of 2 nitrobenzaldehyde. *J Physiol* **555**.**P**, D1.

Soeller C & Cannell MB (1999). Examination of the transverse tubular system in living cardiac rat myocytes by 2-photon microscopy and digital image-processing techniques. *Circ Res* **84**, 266–275.

Spitzer KW, Ershler PR, Skolnick RL & Vaughan-Jones RD (2000). Generation of intracellular pH gradients in single cardiac myocytes with a microperfusion system. *Am J Physiol Heart Circ Physiol* **278**, H1371–1382.

Spitzer KW, Skolnick RL, Peercy BE, Keener JP & Vaughan-Jones RD (2002). Facilitation of intracellular H^+ ion mobility by CO_2/HCO_3^- in rabbit ventricular myocytes is regulated by carbonic anhydrase. *J Physiol* **541**, 159–167.

Stewart AK, Boyd CAR & Vaughan-Jones RD (1999). A novel role for carbonic anhydrase: pH gradient dissipation in mouse small intestinal enterocytes. *J Physiol* **516**, 209–217.

Swietach P, Leem CH, Spitzer KW & Vaughan-Jones RD (2005*a*). Experimental generation and computational modelling of intracellular pH gradients in cardiac myocytes. *Biophys J* **88**, 3018–3037.

Swietach P, Spitzer KW & Vaughan-Jones RD (2005*b*). Local release of caged protons by UV flash photlysis as a means of producing intracellular pH non-uniformity. *FASEB J* **19**, A146.

Swietach P & Vaughan-Jones RD (2005). Spatial regulation of intracellular pH in the ventricular myocyte. *Ann N Y Acad Sci* **1047**, 271–282.

Swietach P, Zaniboni M, Stewart AK, Rossini A, Spitzer KW & Vaughan-Jones RD (2003). Modelling intracellular H^+ ion diffusion. *Prog Biophys Mol Biol* **83**, 69–100.

Thomas JA, Buchsbaum RN, Zimniak A & Racker E (1979). Intracellular pH measurements in Ehrlich ascites tumor cells utilising spectroscopic probes generated in situ. *Biochemistry* **18**, 2210–2218.

Vanysek P (1999). Ionic conductivity and diffusion at infitine dilution. In *CRC Handbook of Chemistry and Physics*, 79th edn, section 5, Thermochemistry, electrochemistry and kinetics, ed. Linde DR, pp. 93–95. CRC Press, London.

Vaughan-Jones RD, Peercy BE, Keener JP & Spitzer KW (2002). Intrinsic H^+ ion mobility in the rabbit ventricular myocyte. *J Physiol* **541**, 139–158.

Vaughan-Jones RD, Spitzer KW & Swietach P (2006). Spatial aspect of intracellular pH regulation in cardiac myocytes. *Prog Biophys Mol Biol* (in press).

Zaniboni M, Swietach P, Rossini A, Yamamoto T, Spitzer KW & Vaughan-Jones RD (2003). Intracellular proton mobility and buffering power in cardiac ventricular myocytes from rat, rabbit, and guinea pig. *Am J Physiol Heart Circ Physiol* **285**, H1236–1246.

Acknowledgements

We thank the British Heart Foundation for funding this work (Programme Grant to R. D. Vaughan-Jones). We also thank the Wellcome Trust (scholarship to P. Swietach) and Overseas Research Scheme, UK (to P.S.). We thank Kenneth W Spitzer for providing samples of double-barrelled, square-bore glass capillaries for the fabrication of the dual microperfusion apparatus. We also thank Ms Nurindura Banger (BHF Programme Grant funding) for first-class technical assistance.

Supplemental material

The online version of this paper can be accessed at:
DOI: 10.1113/jphysiol.2005.086165
http://jp.physoc.org/cgi/content/full/jphysiol.2005.086165/DC1 and contains supplemental material detailing the H^+: diffusion-reaction model, plus a mathematical analysis supporting the pH: insensitivity of P_{SNARF}.
This material can also be found as part of the full-text HTML version available from http://www.blackwell-synergy.com